Available online at www.sciencedirect.com

ScienceDirect

International Journal of Solids and Structures 45 (2008) 3074–3087

INTERNATIONAL JOURNAL OF SOLIDS AND STRUCTURES

www.elsevier.com/locate/ijsolstr

Localization and propagation of curvature under pure bending in steel tubes with Lüders bands

Stelios Kyriakides [a,*], Ali Ok [a], Edmundo Corona [b]

[a] *Research Center for Mechanics of Solids, Structures & Materials, WRW 110, The University of Texas at Austin, Austin, TX 78712, USA*
[b] *Department of Aerospace and Mechanical Engineering, University of Notre Dame, Notre Dame, IN 46556, USA*

Received 3 December 2007
Available online 18 January 2008

Abstract

The paper examines the plastic bending of steel tubes exhibiting Lüders bands through a combination of experiments and analyses. In pure bending experiments on tubes with diameter-to-thickness ratio of 18.8 tested under end-rotation control, following the elastic regime the moment initially traced a somewhat ragged plateau. At the beginning of the plateau Lüders bands appeared on the tension and compression sides of the cross section and simultaneously the curvature localized in one or two short zones while the rest of the tube maintained a much lower curvature. As the rotation of the ends was increased, one of the higher curvature zones spread at a nearly steady rate, affecting an increasingly larger part of the tube. When the whole tube was deformed to the higher curvature, the moment started to gradually increase while the tube deformed uniformly. A moment maximum was eventually attained and the structure failed by localized diffuse ovalization without any apparent effect from the initial Lüders bands-induced propagating instability. The problem was analyzed using 3D finite elements with a fine mesh. The material was modeled as an elastic–plastic solid with an up–down–up response over the extent of the Lüders strain, followed by hardening. The calculated response reproduced all major structural events observed experimentally including the initiation of the Lüders deformation, the moment plateau that followed, its extent, and the curvature localization and propagation associated with it. As in the experiments, once the high curvature extended over the whole tube length, the response of the tube became stable and the curvature uniform. With further bending the increasing ovalization induced a limit moment at a very high curvature.

Keywords: Bending of pipe; Lüders bands; Localization

1. Introduction

An efficient way of installing pipelines offshore is the so-called reel-lay method. This consists of winding several miles of line onto a large diameter reel mounted on a sea going vessel at a coastal fabrication facility. The vessel then travels to the installation site offshore where the line is unwound, straightened and paid into

* Corresponding author.
E-mail address: skk@mail.utexas.edu (S. Kyriakides).

0020-7683/$ - see front matter © 2008 Elsevier Ltd. All rights reserved.
doi:10.1016/j.ijsolstr.2008.01.013

the ocean, finally resting on the sea floor. The process induces bending strains of the order of 2–3%, which must be sustained while guaranteeing the geometric integrity of the pipe. In addition to pipeline applications, cold bending of tubes is a common practice in the manufacture of various components in the aerospace, automotive, nuclear and other industries and therefore, the problem is reasonably well understood. Briefly, bending tends to ovalize the tube cross-section (Brazier, 1927). Ovalization reduces the bending rigidity and leads to a limit load instability associated with local collapse. For thinner tubes the limit load is preceded by wrinkling that precipitates local collapse by kinking (see Ju and Kyriakides (1991, 1992), Kyriakides and Ju (1992), and Kyriakides and Corona (2007) and their references). In the case of reel-lay, given the reel and pipe diameters, the integrity of the structure is ensured by judicious choice of the pipe wall thickness.

Plastic bending can be further complicated when the pipe steel exhibits Lüders banding, a material instability associated with unpinning of dislocations from nitrogen and carbon atmospheres. The phenomenon is common in low-carbon steel seamless pipe that is hot finished and takes place in the initial part of the plastic regime of the material (see review in Hall (1970)). The macroscopic effect of Lüders banding is localized deformation. For example, in a uniaxial test on a strip it manifests as inclined bands of plasticized material that propagate from one end of the strip to the other while the stress remains unchanged (see Fig. 3 in Kyriakides and Miller (2000)). During the propagation of the fronts, Lüders deformed material co-exists with material still in the elastic range. At the termination of the stress plateau, which typically extends over a strain of 1–3%, the material starts to harden and the deformation becomes homogeneous once more. In the case of pipe under bending, this material instability interacts in a complex manner with structural effects such as ovalization, wrinkling and other instabilities and influences the extent to which the integrity of the pipe can be maintained.

This complex interaction was demonstrated in the bending experiments of Aguirre et al. (2004) on tubes with diameter-to-thickness ratio (D/t) of 27.2 that had two different levels of Lüders strain. The moment–curvature responses recorded under pure bending exhibited an initial linearly elastic regime that terminated into a moment plateau via a relatively sharp transition knee. Wrinkles of various wavelengths appeared on the compressed side soon after the onset of inelastic deformation while, simultaneously, narrow Lüders bands emanated from the wrinkles. The bands were straight and oriented at $\pm(45–55°)$ to the axis of the tube. As bending progressed, the wrinkle amplitude grew and the bands lengthened, broadened and multiplied. The tubes eventually collapsed by local buckling induced by the wrinkles. The curvature at collapse was found to depend on the extent of the Lüders strain, with larger Lüders strain causing earlier collapse.

In more recent experiments we have found the interaction of Lüders bands and structural nonlinearities to be strongly influenced by the tube D/t. In this paper we report a new phenomenon that was observed to occur for tubes with $D/t = 18.8$. The relatively low D/t suppresses the growth of wrinkles and simultaneously enables the tube to retain its geometric integrity past the bending deformation regime dominated by Lüders banding. This characteristic results in a unique two-curvature deformation regime for part of the bending history.

Aguirre et al. (2004) showed that adoption of an up–down–up elastic–plastic response for the steel enables simulation of the moment plateau recorded in the experiments as well as reproduction of the x-shaped banded localized patterns that emanate from wrinkle peaks. Similar partially unstable constitutive models are adopted here to simulate the phenomena of the present problem.

2. Experimental

2.1. Experimental facilities

The bending experiments involved carbon steel (CS) 1020 seamless tubes with a nominal diameter (D) of 1.25 in and a D/t of approximately 18.8. Several tubes were cut to the required length and heat-treated in a vacuum furnace. The temperature was ramped up to 700 °C in 60 min, it was held constant for 40 min followed by slow furnace cooling. The engineering stress–elongation (strain) response of the heat-treated material was measured using an axial strip extracted from the end of the tube specimen. In the case shown in Fig. 1, heat treatment reduced the yield stress (σ_L) of the alloy to 31.4 ksi (217 MPa) and introduced Lüders bands of $\Delta\varepsilon_L = 1.84\%$. At the termination of the stress plateau the response exhibits hardening reaching an ultimate stress of approximately 50 ksi (345 MPa).

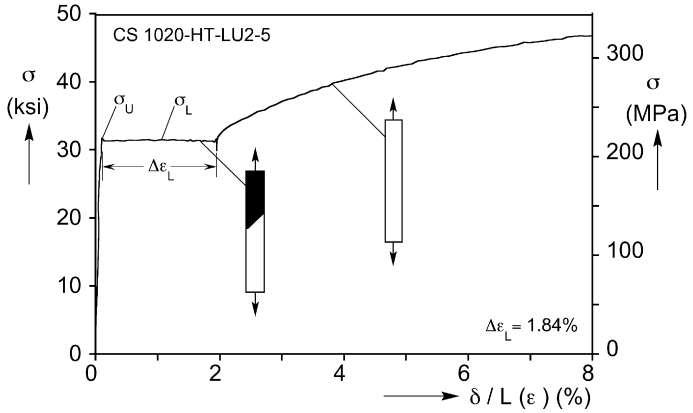

Fig. 1. Stress–elongation response of heat-treated steel exhibiting Lüders deformation of 1.84% followed by hardening.

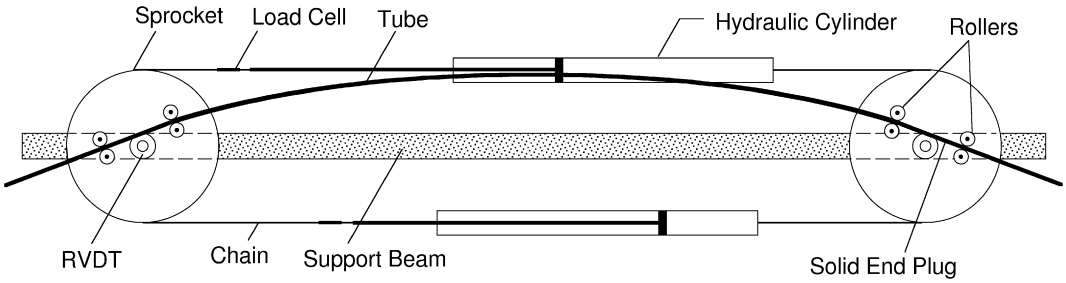

Fig. 2. Schematic showing the pure bending testing facility used in the experiments.

The heat-treated tubes were bent to failure in the custom four-point bending facility shown in Fig. 2 (Corona and Kyriakides, 1988). The bending machine consists of two free-turning sprockets mounted on two stiff support beams. Heavy chains run around the sprockets and are connected to two actuators and in-line load cells to form a closed-loop. Solid steel extension rods are closely fitted into each end of the tube and the assembly is mounted onto the bending machine. The solid rods engage smooth rollers housed in each sprocket assembly as shown in the figure. The machine is activated by contracting one of the cylinders and simultaneously extending the other, in the process rotating the sprockets and the solid rods. The roller arrangement allows an essentially four-point bending loading of the tube as well as the required inward translation of the rods. In the present tests, the tubes had to be bent monotonically to relatively high curvatures. Additional rotation capacity was provided by setting one of the actuators (stroke = 11 in–279 mm) in the fully extended position and the second in the fully contracted position.

The applied moment (M) is monitored by the in-line load cells shown in Fig. 2, and rotary transducers (RVDTs) record the rotation of the sprockets (θ_α, $\alpha = 1, 2$). While the deformation of the tube is uniform, its curvature (κ) is proportional to the sum of the angles of rotation of the two sprockets. The outputs of the instruments are monitored through a computer-operated data acquisition system programmed to sample them whenever any one signal $\{M, \theta_1, \theta_2\}$ changes by a preset amount. (We point out that the bending curvatures of the current experiments exceeded the design capacity of the bending machine. Consequently, factors that in normal operating conditions have small effect and are neglected had to be considered and the data appropriately corrected. The main of these factors is the effect of the weight of the relatively long solid rods required on the moment. In addition, at large sprocket rotations the small friction in the rollers has some effect on the moment; this was measured and corrected for.) In the particular experiments reported here, the tubes developed inhomogeneous bending deformation for part of the bending history. In lieu of other possible deformation monitoring techniques, the tube global deformation was continuously monitored with a video camera. In addition, full-field views of the deforming tube were recorded at regular intervals using a high-resolution digital camera.

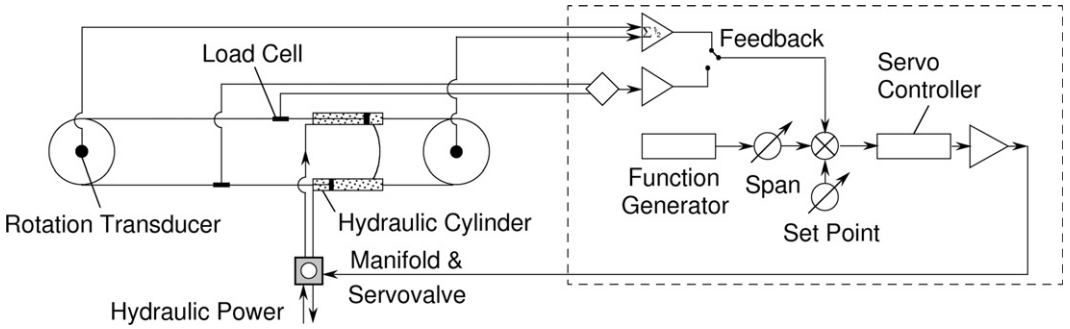

Fig. 3. Schematic of the closed-loop controller of the bending device operating in rotation control.

The bending machine is operated by a closed-loop, servo-controlled system shown schematically in Fig. 3 that allows a choice of either moment or rotation control (for more on performance see Corona and Kyriakides (1991)). The present experiments were run under rotation control at a rate that corresponds to a maximum bending strain rate of $1 \times 10^{-4}\,s^{-1}$.

2.2. Experimental results

Results from two experiments on tubes with the geometric and material parameters listed in Table 1 will be reported. The first experiment involved a tube with an effective length of $2L = 18.2D$ (effective length is the length of tube between the ends of the solid rod inserts). Fig. 4 shows the measured moment vs. the average of the two rotations recorded by the RVDTs, $\bar{\theta}_L$. Thus, when the tube deformation is uniform the curvature of the tube is given by $\kappa = \bar{\theta}_L/L$. The moment is normalized by the fully plastic moment $M_o(= \sigma_L D_o^2 t)$ and the average rotation by $Lt/D_o^2(\equiv L\kappa_1)$. Fig. 5 shows a set 14 full-span photographs of the tube that correspond

Table 1
Major geometric and material parameters of tubes tested

Exp. No.	D in (mm)	t in (mm)	D/t	$2L/D$	E Msi (GPa)	σ_L ksi (MPa)	$\Delta\varepsilon_L\%$
LU2-5	1.252 (31.81)	0.0668 (1.70)	18.74	18.2	27.7 (191)	31.4 (217)	1.84
LU2-2	1.252 (31.81)	0.0663 (1.69)	18.88	14.4	29.1 (200)	30.2 (208)	1.8

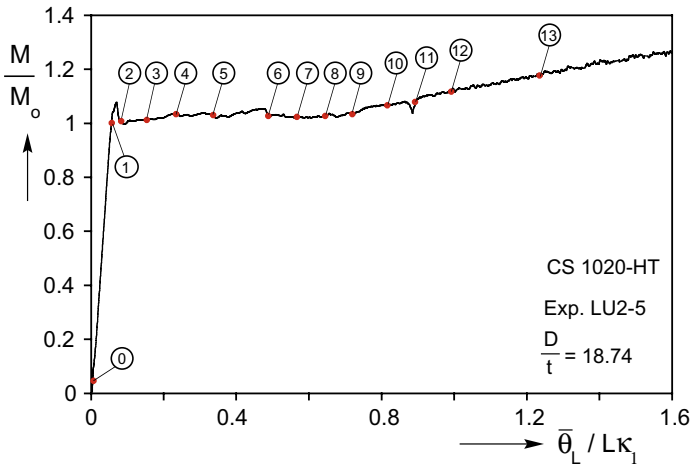

Fig. 4. Measured moment vs. average end rotation for a tube with $D/t = 18.8$ (Exp. LU2-5).

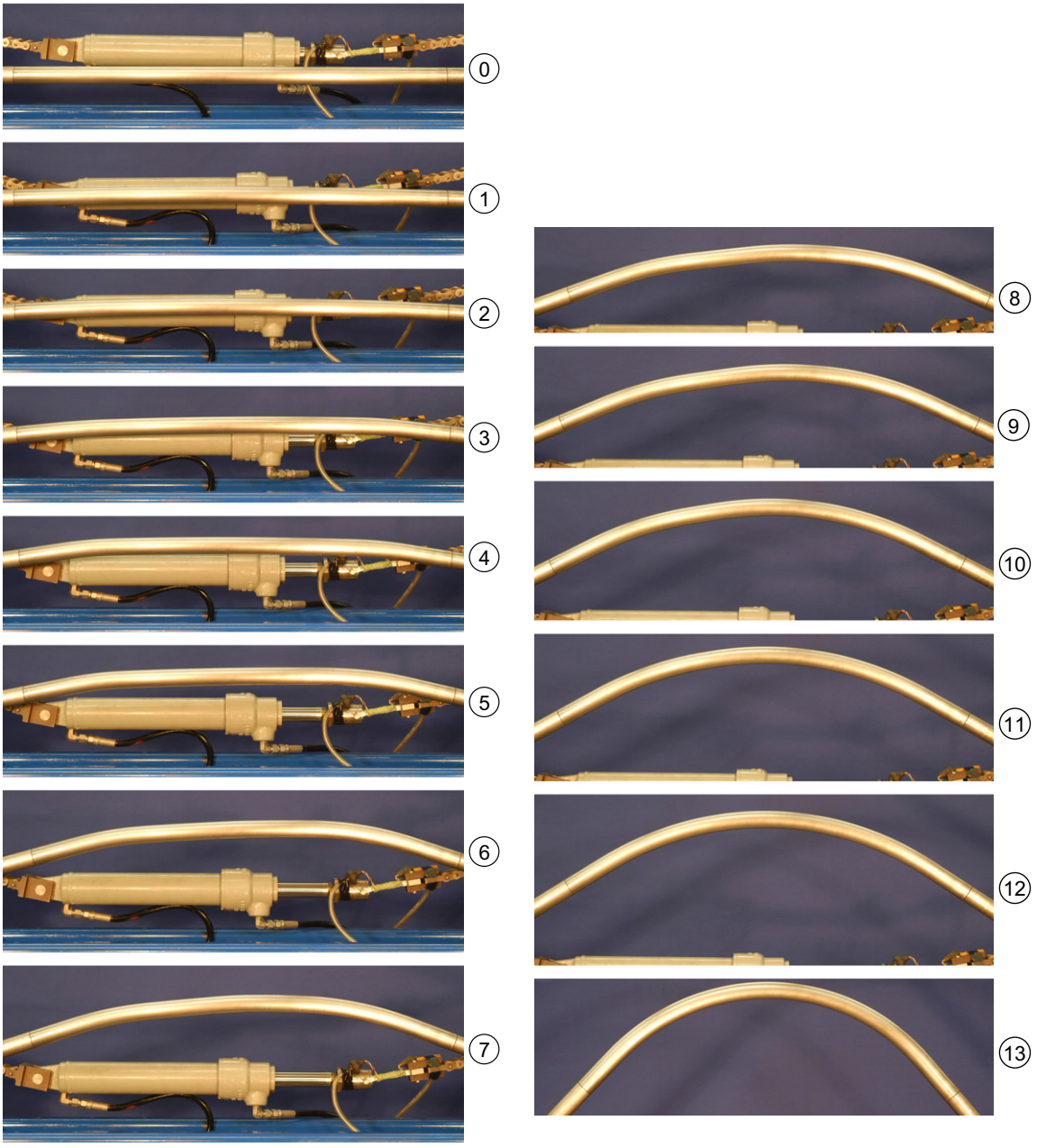

Fig. 5. Sequence of bent tube configurations corresponding to the response in Fig. 4. Configurations ②–⑩ show first localization of curvature and then spreading of the higher curvature zones.

to the initial configuration (⓪) and 13 subsequent ones that show the tube at different stages of bending. The photographs correspond to the locations marked on the response with numbered solid bullets.

The response exhibits an initial stiff and linear behavior corresponding to the linearly elastic regime of the material. The tube bends uniformly, as confirmed by configuration ① in Fig. 5, with the expected bending rigidity of EI ($I \equiv$ 2nd moment of area of the cross section about the neutral axis). The moment attains a local maximum of $M = 1.076M_o$ and then drops sharply down to a value that is close to M_o, where it starts to trace a somewhat ragged moment plateau. It is interesting to observe that some nonlinearity in the response was recorded just prior to the moment maximum, indicating that some Lüders banding had initiated. Most prob-

ably this occurred in the regions just adjacent to the ends of the solid rods where small stress concentrations are unavoidably present. The moment drop is a definite sign that an instability has taken place. Lüders deformation nucleates in the form of bands that are inclined to the axis of the tube on the top and bottom surfaces as described in Aguirre et al. (2004). The first nucleation is adjacent to the LHS solid rod insert in configuration ②. Apparently, the Lüders deformation affected enough of the tube cross-section to cause a zone approximately $2D$ long to bend more than the rest of the tube, in other words bending localized (note that the solid rods penetrate $3.2D$ into the end of the tubes). As the end-rotation continues to increase, the moment recovers slightly and then remains nearly constant, hovering around M_o. By configuration ③ Lüders banding and localized bending have initiated at a site adjacent to the RHS solid insert; so now two zones of higher curvature co-exist with the middle section of the tube having the visibly smaller curvature of approximately M_o/EI. In configuration ④ the curvature in the zones on the left and right has increased further and subsequently the higher curvature domain starts to propagate from the site on the right towards the center of the tube. It appears that the rightward propagation commences after the small moment peak at bullet ④. In configuration ⑤ the length of the high curvature zone on the right has increased significantly and to a smaller extent on the left. Between location ⑤ and ⑥ the moment rose slightly and then dropped back to about M_o. Such events are associated with re-initiation of the propagation of a previously stagnant front in this case from the site on the left. Consequently, in configurations ⑥–⑨ the high curvature domains propagate from the two sites towards the center of the tube, although the front on the right is clearly moving faster than the one on the left. By configuration ⑨ most of the tube has attained the high curvature with only a short section to the left of center maintaining a smaller curvature. At this point the moment starts a gradual rise while the curvature is increasing essentially everywhere. Yet, judging from configuration ⑩, a short section to the left of center still maintains a lower curvature than that of the sections to the left and right of it. Apparently, this zone requires a higher moment to undergo the Lüders deformation, so the moment gradually rises to $1.08\ M_o$. This persistent zone finally deforms to the same curvature as the rest if the tube and when this happens the two propagating fronts meet causing a sharp dip in the moment. Dips in the driving "force" of such propagating instabilities are commonly observed when two fronts meet (see for example results from tensile tests on steels that experience Lüders banding in Butler (1962) and Kyriakides and Miller (2000); similar load dips were observed during stress-induced phase transformations in shape memory alloy wires and strips in Shaw and Kyriakides (1995, 1997)) Beyond the moment dip the moment increases monotonically, and the tube deforms uniformly as seen in configurations ⑪–⑬. The rotation capacity of the testing facility was reached soon after configuration ⑬, and the test was terminated before the expected moment maximum and the ensuing diffuse localized ovalization could develop.

Returning to the moment plateau, the curvature at the termination of the plateau approximately corresponds to the curvature of the localization induced by Lüders banding. The moment dip just prior ⑪ occurred at a curvature of $\kappa = 0.887\kappa_1$. By contrast, the end of the Lüders stress plateau in the uniaxial tension test occurred at a strain of 0.0195. If we take this as the strain of the outermost fibers of the tube during bending, it translates into a curvature of $0.657\kappa_1$, which is smaller than the value at the end of the moment plateau. This difference indicates that for bending localization triggered by the Lüders deformation to take place, more than just the fibers further from the neutral axis of the tube must be involved.

The events observed during the tracing of the moment plateau are reminiscent of those that occur in other solids and structures that undergo propagating instabilities (see reviews in Kyriakides (1994, 2001)). Each problem in the family is characterized by an instability that leads to localized deformation. Each also has an inherent feature that limits the extent to which localized deformation can grow; in other words, localization is arrested at some stage. Under prevailing conditions the locally weakened zone can spread (propagate) to the rest of the structure, which was not affected by the initial local instability. The propagation can be dynamic but in most cases, under "displacement-controlled" loading, steady-state quasi-static propagation can be achieved. As this takes place, the "load" remains essentially unchanged and highly deformed and relatively undeformed phases co-exist. In the present problem the prevalent instability is Lüders banding that causes localized bending in the tube as evidenced in configurations ②–④ in Fig. 5. The extent of the deformation of the Lüders bands is limited (in this case $\Delta\varepsilon_L = 1.84\%$), and this consequently limits the curvature of the induced localized bending. If bending is halted after, say configuration ③, most of the structure will unload elastically, but two permanently bent zones at the two ends will be left behind. Under the end-rotation loading of the experiment,

the Lüders affected higher curvature regions spread quasi-statically at a nearly constant moment. During this propagation, highly bent and less bent zones coexisted. When the whole tube was deformed to the higher curvature, the instability had run its course and subsequently the structure returned to uniform deformation, in this case to constant curvature.

The post-Lüders banding events that lead to the collapse of the tube were illustrated in a second experiment on a tube of similar geometry that was heat-treated in the same manner (major geometric and material parameters listed under LU2-2 in Table 1). The main difference was that in this case the test specimen was shorter than the one in the previous experiment. An effective length of $2L = 14.4D$ enabled bending to a higher curvature, allowing the tube to attain its natural limit moment. The moment–curvature response of this case is shown in Fig. 6. The initial parts of the response including the linearly elastic regime, the moment plateau, and the subsequent stable response are very similar to those of the previous experiment. During the moment plateau, localized curvature developed that gradually spread covering the whole specimen, while beyond the plateau the tube deformed uniformly. (We observe that the location of the initial localization as well as the direction of propagation of the fronts were not the same in the two experiments.) Bending-induced ovalization to the tube cross section is responsible for the gradual reduction of the bending rigidity of the tube (see Fig. 6), leading eventually to a moment maximum at a curvature of $\kappa = 2.08\kappa_1$ (marked on the response with a caret "∧").

The rotation-controlled loading enabled tracking the response beyond the moment maximum. The moment is seen to drop with end-rotation and simultaneously diffuse localized ovalization developed, which can be seen in the photograph in Fig. 7 to affect a region about $6D$ long around the center of the specimen (photograph taken at the termination of the test). Continued rotation of the ends would have resulted in a sharpening of the localization into a local kink. For all intents and purposes the curvature at the second moment-maximum can be considered as the collapse curvature of the tube.

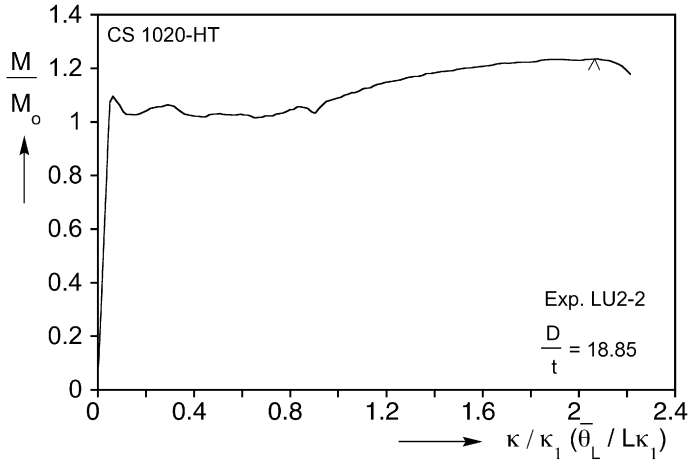

Fig. 6. Moment vs. average end-rotation recorded for a tube with $D/t = 18.8$ (Exp. LU2-2) that collapsed by diffuse localized ovalization.

Fig. 7. Post-testing photograph of the tube used in Exp. LU2-2 showing localized ovalization at mid-span.

In both experiments small amplitude wrinkles were observed to develop in the zones of localized curvature during the tracing of the moment plateau. Their amplitude did not grow significantly with curvature and their influence on the eventual failure of the tube was deemed not significant. Overall, the post-Lüders banding part of the response is similar to that observed previously to occur for thicker tubes with monotonic stress–strain responses (see Kyriakides and Ju (1992) and review in Kyriakides and Corona (2007)). Indeed, it is clear that once the tube entered the stable regime past the moment plateau, the effect of the previous localized bending and its propagation was minimal, if any, as no permanent effect of these events was observed.

3. Analysis

Lüders banding is a dislocation governed material instability, which macroscopically manifests as discontinuous deformation (see Cottrell and Bilby (1948), Lomer (1952), Johnston and Gilman (1959), Butler (1962), Hall (1970)). Kyriakides and Miller (2000) showed that the major events induced by Lüders banding in uniaxial, quasi-static tension tests on steel strips such as inclined higher deformation bands that propagate at a nearly constant load, could be simulated numerically by the adoption of a non-monotonic, elastic–plastic stress–strain response. Its main characteristic was an up–down–up shape over the Lüders strain regime; in other words, the material was assumed to be unstable for part of its deformation history.

Aguirre et al. (2004) used a similar constitutive model in a finite element model with a fine mesh to capture the initiation and propagation of Lüders bands in a short section of a tube with $D/t = 27.2$ under pure bending (see also Corona et al. (2002)). Because of the relatively high D/t of their tubes, the structural response and associated events were governed by an interaction of wrinkling with Lüders banding. They were also able to reproduce the structural response as well as the local events observed quite well.

The present problem is different in that because of the much lower tube D/t, wrinkling does not influence the observed events, and the structure maintains its integrity past the Lüders affected bending deformation. Indeed, it eventually failed by localized diffuse ovalization much like a tube of the same geometry but with a monotonic stress–strain response. Furthermore, as Lüders affected deformation progressed, two-curvature regimes were observed to co-exist at the same moment. We will therefore adopt a similar unstable constitutive model as Aguirre et al. but will analyze a much larger domain in order to capture both the initial Lüders-induced localization as well a the subsequent ovalization-induced limit load.

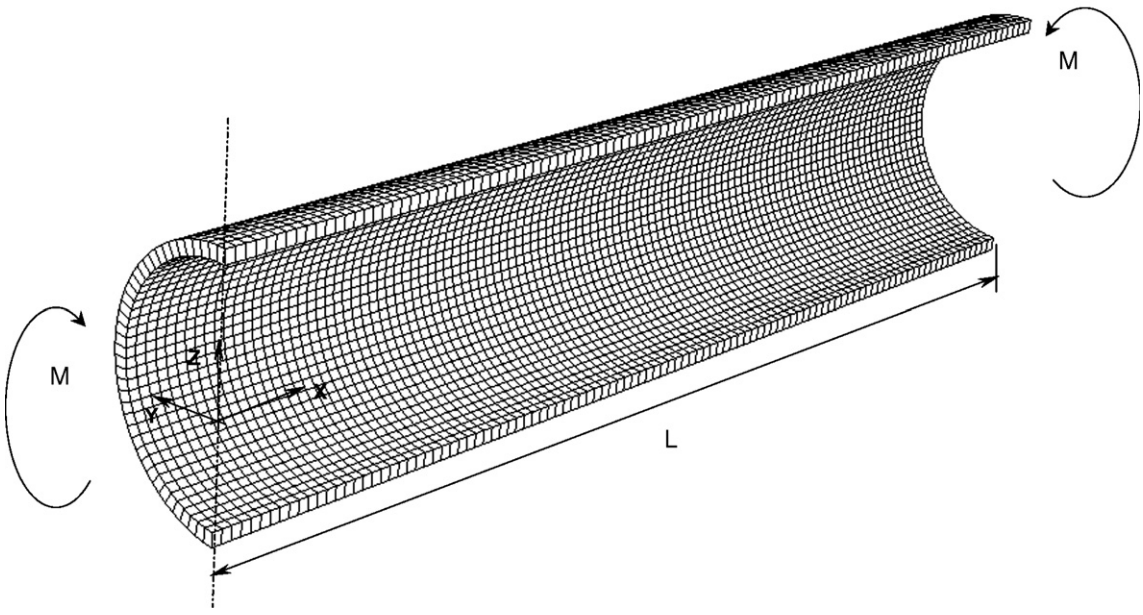

Fig. 8. Finite element mesh used to analyze the problem.

3.1. Model geometry

We consider a section of tube of radius R, wall thickness t and length $2L$ under pure bending. We assume symmetry about the mid-span (plane $y-z$) and about the plane of bending $x-z$. Therefore, consideration of one-quarter of the tube suffices (see Fig. 8). In order to facilitate the development of the expected localization, the domain is chosen to have a length of $L = 14R$. A small geometric imperfection in the form of a linearly varying initial ovality is introduced to the model as follows:

$$w_o = -R\Delta_o\left(1-\frac{x}{L}\right)\cos 2\phi, \tag{1}$$

where w is the displacement in the radial direction and ϕ is the polar angle. The tube is bent by prescribing the angle of rotation at $x = L$, θ_L. This end is constrained to remain plane, while the cross section is free to ovalize by imposing the following multi-point constraint:

$$\tan\theta_L = \frac{x_{\text{ref}} - x_i}{z_{\text{ref}} - z_i}, \tag{2}$$

where (x_i, z_i) are the coordinates of the ith node in this plane and $(x_{\text{ref}}, z_{\text{ref}})$ are those of a reference node (e.g., the bottom or central node). The moment is calculated at the plane of symmetry ($x = 0$) from

$$M = 2\sum_{i=1}^{N} z_i F_i \tag{3}$$

where F_i is the axial force acting on the ith node of the cross section and z_i is its distance from the axis of the tube.

Lüders deformation results in inhomogeneous deformation with jumps in strain of the order of the Lüders strain. We have found ABAQUS's incompatible elements C3D8I to be best suited for this type of problem, although other alternatives were found to yield acceptable results as well. These are linear elements enhanced to allow for jumps in the deformation gradient inside the element while displacement continuity is maintained (based on Simo and Armero (1992); see also Ortiz et al. (1987) and Nacar et al. (1989), Wilson et al. (1973)). We have used one element through the thickness of the tube, 40 around the half circumference and 106 along the length.

3.2. Constitutive model

The material was modeled as a finitely deforming elastic–plastic solid with the engineering stress–strain response shown in Fig. 9. It consists of a linear elastic branch (①–②) that corresponds to the measured elastic

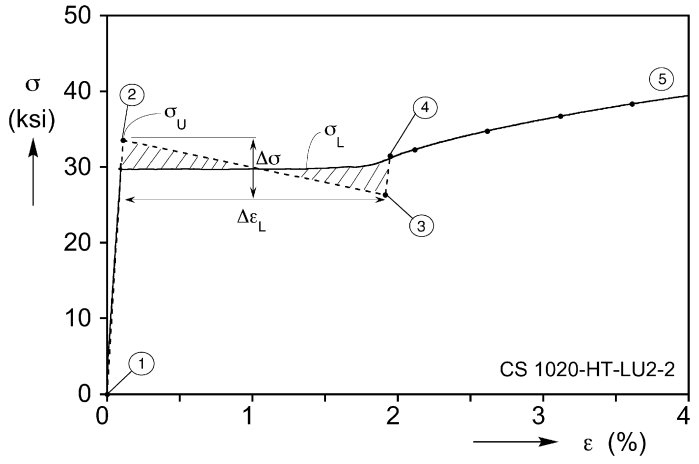

Fig. 9. Measured material response and engineering stress–strain response adopted (dashed line).

modulus. The elastic branch terminates at ② at a yield stress that is approximately $\Delta\sigma/2$ higher than the plateau (σ_L) of the measured response. It is followed by a linear softening branch (②–③), which in turn is followed by a second linear section with positive slope (③–④). The stress levels at points ② and ③ are selected such that the areas of the shaded triangles are equal (i.e., σ_L approximately corresponds to the Maxwell stress). The hardening part of the measured stress–strain response beyond point ④ is represented by a piecewise linear fit.

3.3. Results

The case analyzed corresponds to Exp. LU2-2 in Table 1. The stress–strain response used is the one in Fig. 9 where the slope of the negative branch (②–③) was taken as −400 ksi (2.76 GPa) and an imperfection amplitude of $\Delta_o = 0.003$ was adopted. Fig. 10 shows the early part of the calculated moment-end rotation response along with the corresponding experimental one. The calculated response is seen to be in good agreement in all aspects with the measured results, i.e., the initial onset of instability, the moment plateau, its extent, and the subsequent stable branch. Nine deformed configurations of the quarter-tube analyzed corresponding to the numbered bullets on the response are shown in Fig. 11. In configuration ①, which corresponds to $\theta_L/L\kappa_1 = 0.059$, just before the local moment maximum, the tube is bent uniformly. To illustrate this point the slope, $\theta(s)$, calculated from nodal displacements along the original mid-surface of the tube, is plotted against the natural coordinate s in Fig. 12. The plane $s = 0$ is a plane of symmetry and thus $\theta(0) = 0$. The free end of the tube ($s = L$) undergoes the maximum rotation $\theta(L) = \theta_L$. Thus, when the tube deforms uniformly $\theta(s)$ grows linearly between 0 and θ_L. This in fact is the case for configuration ①.

The local moment maximum at the end of the linearly elastic range indicates that Lüders banding initiates, in this case near the plane of symmetry ($s = 0$). This takes the form of inclined bands on the top and bottom surfaces of the tube as described in Aguirre et al. (2004). By configuration ② in Fig. 11 the Lüders banding has led to the formation of a higher curvature zone close to the plane of symmetry on the LHS while the rest of the domain has smaller curvature. The localization of bending is clearly seen in Fig. 12 where two distinct slopes are joined by a transition region extending over a length approximately one-half of a tube diameter.

In subsequent configurations, as θ_L increases the highly bent zone spreads along the length of the tube while the curvature of the intact part remains essentially unchanged. This is clearly illustrated in configurations ②–⑧ in Fig. 11 and more quantitatively in Fig. 12. In each configuration a transition zone approximately $0.5D$ long joins the high curvature section on the LHS with the low curvature section on the RHS. The low curvature corresponds to the slope $\theta'(s)$ of BC, with a value of $\theta_L/L\kappa_1 = 0.092$. This value corresponds approximately to the calculated local moment maximum preceding the plateau. The high curvature corresponds to the slope $\theta'(s)$ of OA, which has a value of approximately $\theta_L/L\kappa_1 = 0.90$. This corresponds to the small

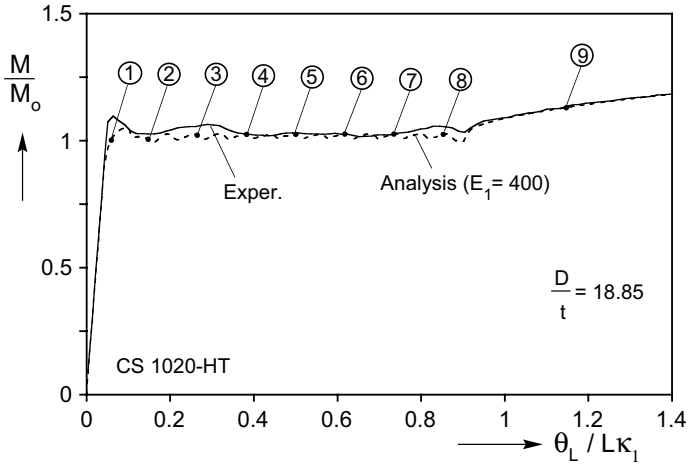

Fig. 10. Comparison of measured and calculated moment vs. average end rotation response (Exp. LU2-2).

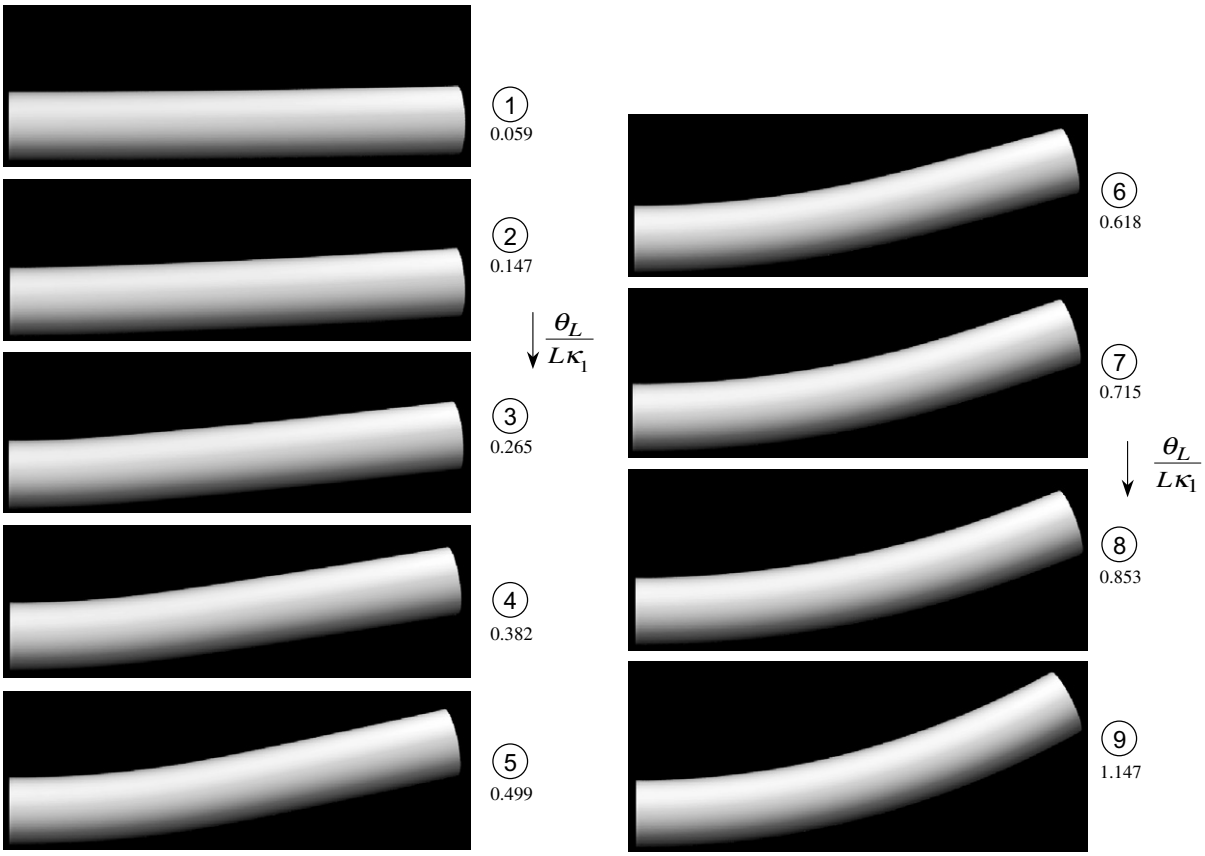

Fig. 11. Sequence of bent tube configurations corresponding to response in Fig. 10. Configurations ②–⑧ show coexistence of two-curvature regimes.

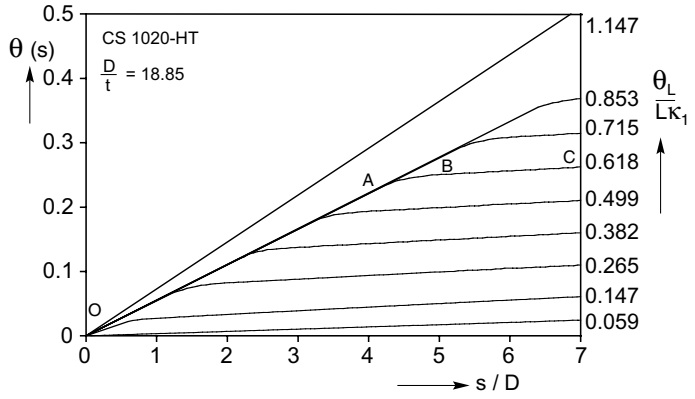

Fig. 12. Calculated local slope ($\theta(s)$) along the length of the tube (s) corresponding to results in Figs. 10 and 11.

moment dip at the end of the calculated moment plateau. As θ_L is increased the zone with the higher curvature propagates to the right consuming eventually the whole length of the tube (soon after configuration ⑧). For $\theta_L/L\kappa_1$ higher than approximately 0.90, the deformation of the tube becomes uniform as illustrated by configuration ⑨ in Fig. 11 and by the linear $\theta(s)$ trajectory for $\theta_L/L\kappa_1 = 1.147$ in Fig. 12. The moment–curvature response now has a positive slope and the curvature is uniform.

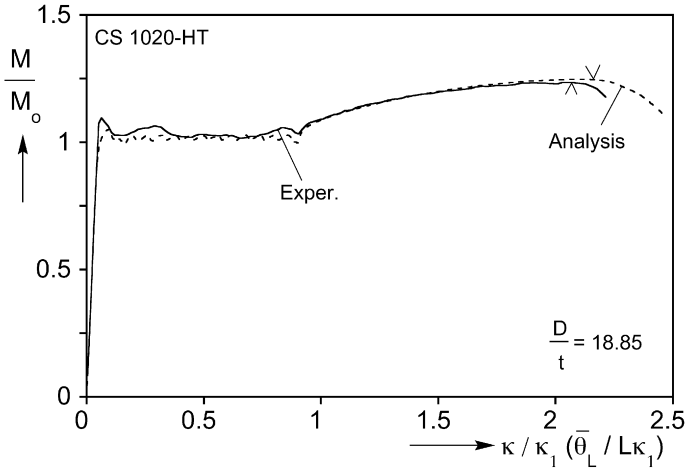

Fig. 13. Comparison of measured and calculated moment vs. average end rotation response for Exp. LU2-2.

Fig. 13 shows an expanded comparison of the measured and calculated moment–curvature response. The stable branch of the calculated response is seen to follow the experimental one very well. The induced ovalization leads to a gradual decrease in bending rigidity and eventually at a curvature of $\kappa = 2.14\kappa_1$ a limit moment develops (marked on the response with the symbol "v"). Beyond the limit moment, deformation localizes in the form of diffuse ovalization, essentially reproducing the experiment. The localized ovalization initially covers a length of about $4D$. Excessive bending tends to sharpen the deformation into a diffuse kink.

In summary, we see that the FE model coupled with the partially unstable material response adopted (Fig. 9) reproduces the two-curvature deformation induced by the Lüders bands over part of the bending history, as well as the subsequent uniform deformation moment–curvature branch. The latter terminates in a limit load instability at a curvature that is close to that recorded in the experiment.

The effect of several model parameters on the results was examined and the results can be outlined as follows. The slope of the unstable branch of the stress–strain response (or alternatively the value of $\Delta\sigma$) is unknown. Aguirre et al. (2004) pointed out that the localized band deformation patterns observed in their experiments could be reproduced numerically provided the material instability was "strong enough," i.e., the slope of the unstable branch of the stress–strain response should exceed a certain value. The same was found to hold for the present problem. In the tensile tests performed on the tube materials, the initial stress peak (upper yield stress) often present for materials that exhibit Lüders bands was masked to some degree by stress concentrations at the gripped ends of the specimens. Thus, the value of $\Delta\sigma$ was selected from past experience, ensuring also that the slope of the negative branch was past the threshold mentioned above. In parametric studies it was found that increasing the value of the negative slope tends to increase the extent of the moment plateau somewhat.

A second issue that was scrutinized is the mesh sensitivity of the solution. Parametric mesh studies showed the main aspects of the solution reported to be converged. During the tracing of the moment plateau the length of the transition zone joining the two-curvature regimes was found to exhibit some sensitivity to the mesh. In this first airing of the problem, and in the first attempt at demonstrating that its main features can be reproduced by the simple up–down–up constitutive model adopted, capturing the exact geometry of the transition region was deemed to be of secondary importance. Thus possible regularization techniques were not pursued.

The effect of the type and amplitude of the initial imperfection adopted on the solution was another parameter examined. The linearly varying imperfection used was a simple way of initiating localization at mid-span. The amplitude of the ovalization used is within the range of measured values and was not found to affect the results in any significant manner.

4. Summary and conclusions

Low-carbon steel tubes and pipes can exhibit Lüders banding in the early stages of plastic deformation. This unstable material regime extends over a strain range of 1–3% and is followed by the usual hardening material behavior. This work is concerned with the effect of the Lüders bands on the plastic bending of tubes including the extent to which the tubes can be deformed. A number of bending experiments were performed on steel tubes with a $D/t = 18.8$ using a material with a Lüders strain of 1.84%. By controlling the rotation of the ends of the tubes it was observed that soon after first yielding the moment traced a somewhat ragged plateau indicating the progression of a nearly steady-state event. At the beginning of the plateau, narrow zones of Lüders bands appeared on the tension and compression sides of the cross section close to the ends of the tubes. Simultaneously, the curvature in these zones localized. Initially, the two higher curvature zones affected only about two tube diameters while the rest of the tube maintained a much lower curvature. As the rotation of the ends of the tubes increased, one of the higher curvature zones gradually spread affecting an increasingly larger part of the tube. This propagation continued with the moment remaining relatively constant until the whole tube was deformed to the higher curvature. This occurred when the two higher curvature zones met causing a temporary, small drop in the moment. Subsequently the tube deformed uniformly with the moment increasing gradually while the cross section ovalization progressively increased. The increase in ovalization led to a gradual decrease in bending rigidity and to the attainment of a moment maximum at a curvature of $2.08\kappa_1$. Beyond the moment maximum the expected diffuse localized ovalization failure developed. In other words, the tube underwent a localized instability for part of its bending history. The instability spread at a constant moment, and subsequently the tube resumed stable bending deformation that did not seem to be affected by the preceding localization. This behavior is reminiscent of several other propagating instability phenomena experienced in structures of larger size (see Kyriakides (1994, 2001)).

This sequence of events is contrasted with that observed in thinner tubes with $D/t = 27.2$ by Aguirre et al. (2004). A similar moment plateau was reported, but the tubes failed by localized kinking before the termination of the plateau. This failure was precipitated by a complex interaction of wrinkling and Lüders banding. In other words, for thinner tubes failure occurs before the bending strain is large enough for the stable branch of the material to become active once more. As a consequence, the coexistence of two-curvature regimes was not observed either.

Returning to reeling of pipe, clearly our pipe with $D/t = 18.8$ is reelable while the one with D/t of 27.2 is not. The main practical question is: given a pipe diameter at what D/t will the pipe survive the bending induced by reeling? Although a definitive answer to this question is not yet possible, the results of these two studies indicate that the extent of the Lüders strain influences the events reported and can play a decisive role in determining the transitional D/t that separates the two behaviors reported.

The thicker wall experiments were simulated using a FE model that was long enough to capture the localized structural instabilities of the problem. The domain was discretized with incompatible solid elements using a fine enough mesh that allows Lüders bands to develop and evolve. The material was modeled as a finitely deforming, J_2 type, elastic–plastic solid while the material instability was represented through an up–down–up stress–strain response constructed so that the Maxwell stress and its extent match the measured stress plateau and Lüders strain. The model was bent by prescribing the rotation of the free ends incrementally. The calculated moment-end-rotation response reproduced the moment plateau and its extent as well as the subsequent stable branch. At the onset of the moment plateau, the bending curvature localized initially over a small region. As the end-rotation increased, the higher curvature zone spread outwards reproducing the coexistence of the two-curvature regimes seen in the experiments. The high curvature zone was deformed to a value that corresponds to the end of the moment plateau while the low curvature one remained at a value that corresponds to the beginning of the plateau. The transition zone that joins the two regions was approximately $0.5D$ long. Once the higher curvature spread to the whole domain, the moment started to increase and subsequently the tube bent with a constant curvature. The induced ovalization eventually led to a limit load instability followed by collapse due to the usual diffuse localized ovalization. In summary, the FE model used coupled with the up–down–up constitutive model adopted reproduced the main features observed experimentally both qualitatively as well as quantitatively.

Acknowledgement

The financial support of the work from a consortium of industrial sponsors under the project Structural Integrity of Offshore Pipelines is acknowledged with thanks.

References

Aguirre, F., Kyriakides, S., Yun, H.D., 2004. Bending of steel tubes with Lüders bands. Int. J. Plasticity 20, 1199–1225.
Brazier, L.G., 1927. On the flexure of thin cylindrical shells and other thin sections. Proc. Royal Soc. London A 116, 104–114.
Butler, J.F., 1962. Lüders front propagation in low carbon steels. J. Mech. Phy. Solids 10, 313–334.
Corona, E., Shaw, J.A., Iadicola, M.A., 2002. Buckling of steel bars with Lüders bands. Int. J. Solids Struct. 39, 3313–3336.
Corona, E., Kyriakides, S., 1988. On the collapse of inelastic tubes under combined bending and pressure. Int. J. Solids Struct. 24, 505–535.
Corona, E., Kyriakides, S., 1991. An experimental investigation of the degradation and buckling of circular tubes under cyclic bending and external pressure. Thin-walled Struct. 12, 229–263.
Cottrell, A.H., Bilby, B.A., 1948. Dislocation theory of yielding and strain ageing of iron. Proc. Physical Soc. 62/I–A, 49–62.
Hall, E.O., 1970. Yield Point Phenomena in Metals and Alloys. Plenum Press, New York.
Johnston, W.G., Gilman, J.J., 1959. Dislocation velocities, dislocation densities, and plastic flow in lithium fluoride crystals. J. Appl. Phys. 30, 129–144.
Ju, G.T., Kyriakides, S., 1991. Bifurcation versus limit load instabilities of elastic–plastic tubes under bending and pressure. ASME J. Offshore Mech. Arctic Eng. 113, 43–52.
Ju, G.T., Kyriakides, S., 1992. Bifurcation and localization instabilities in cylindrical shells under bending: part II predictions. Int. J. Solids Struct. 29, 1143–1171.
Kyriakides, S., 1994. Propagating instabilities in structures. In: Hutchinson, J.W., Wu, T.Y. (Eds.), Advances in Applied Mechanics, vol. 30. Academic Press, Boston, MA, pp. 67–189.
Kyriakides, S. 2001. Propagating instabilities in materials. In: Materials Science for the 21st Century, Society of Materials Science, Japan, vol. 1, pp. 316–325, May 2001.
Kyriakides, S., Corona, E., 2007. Mechanics of Offshore Pipelines: Volume 1 Buckling and Collapse. Elsevier, Oxford, UK, Burlington, MA.
Kyriakides, S., Ju, G.T., 1992. Bifurcation and localization instabilities in cylindrical shells under bending: part I experiments. Int. J. Solids Struct. 29, 1117–1142.
Kyriakides, S., Miller, J.E., 2000. On the propagation of Lüders bands in steel strips. ASME J. Appl. Mech. 67, 645–654.
Lomer, W.M., 1952. The yield phenomenon in polycrystalline mild steel. J. Mech. Phys. Solids 1, 64–73.
Nacar, A., Needleman, A., Ortiz, M., 1989. A finite element method for analyzing localization in rate dependent solids at finite strains. Comp. Meth. Appl. Mech. Eng. 73, 235–258.
Ortiz, M., Leroy, Y., Needleman, A., 1987. A finite element method for localized failure analysis. Comp. Meth. Appl. Mech. Eng. 61, 189–214.
Shaw, J.A., Kyriakides, S., 1995. Thermomechanical aspects of NiTi. J. Mech. Phys. Solids 43, 1243–1281.
Shaw, J.A., Kyriakides, S., 1997. On the nucleation and propagation of phase transformation fronts in a NiTi alloy. Acta Materialia 45, 683–700.
Simo, J.C., Armero, F., 1992. Geometrically non-linear enhanced strain mixed methods and the method of incompatible modes. Int. J. Numerical Meth. Eng. 33, 1413–1449.
Wilson, E.L., Taylor, R.L., Doherty, W.P., Ghaboussi, J., 1973. Incompatible displacement models. In: Fenves, S.J. et al. (Eds.), Numerical and Computer Models in Structural Mechanics. Academic Press, New York.